

# SU(2)-invariant spin-1/2 Hamiltonians with RVB and other valence bond phases

K. S. Raman<sup>1</sup>, R. Moessner<sup>2</sup> and S. L. Sondhi<sup>1</sup>

<sup>1</sup>*Department of Physics, Princeton University, Princeton, NJ 08544, USA and*

<sup>2</sup>*Laboratoire de Physique Théorique de l'Ecole Normale Supérieure, CNRS-UMR8549, Paris, France*

(Dated: March 23, 2022)

We construct a family of rotationally invariant, local,  $S=1/2$  Klein Hamiltonians on various lattices that exhibit ground state manifolds spanned by nearest-neighbor valence bond states. We show that with selected perturbations such models can be driven into phases modeled by well understood quantum dimer models on the corresponding lattices. Specifically, we show that the perturbation procedure is arbitrarily well controlled by a new parameter which is the extent of decoration of the reference lattice. This strategy leads to Hamiltonians that exhibit i)  $Z_2$  RVB phases in two dimensions, ii)  $U(1)$  RVB phases with a gapless “photon” in three dimensions, and iii) a Cantor deconfined region in two dimensions. We also construct two models on the pyrochlore lattice, one model exhibiting a  $Z_2$  RVB phase and the other a  $U(1)$  RVB phase.

## I. INTRODUCTION

Just over thirty years ago Anderson<sup>1</sup> introduced the resonating valence bond (RVB) state as an alternative to Néel ordering in antiferromagnets with strong quantum fluctuations. In essence, he proposed that on a sufficiently frustrated lattice an  $S = 1/2$  system would exhibit a disordered state at  $T = 0$ , which would be captured by a wavefunction of the form

$$|\psi\rangle = \sum_c A_c |c\rangle \quad (1.1)$$

where  $|c\rangle$  is a configuration of singlet pairings of spins or valence bonds (Fig 1). For sufficiently short-ranged valence bonds this describes, in contrast to the Néel state, a state with short-ranged spin correlations.

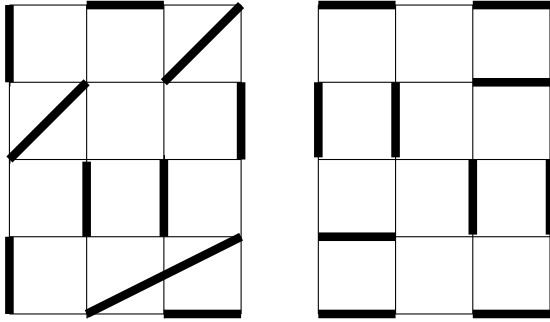


FIG. 1: Sample valence bond configurations. The thick lines represent singlet pairings. The original formulation allowed for bonds of arbitrary length (left). Considerable progress has been made by restricting to configurations with only nearest-neighbor valence bonds (right).

The discovery of the cuprates and the suggestion that their superconductivity could be traced to RVB physics<sup>2</sup> greatly energized the elucidation of the RVB idea and by now a rather complete understanding of its internal logic has emerged. In modern parlance, an RVB

phase is a topological phase, characterized by excitations with fractional quantum numbers and a low energy gauge structure which mediates topological interactions among the excitations<sup>3</sup>. The excitations include *spinons*, the  $S = 1/2$  excitations produced by breaking a valence bond, as well as collective excitations within the valence bond manifold (see figure 2). The sr-RVB<sup>4</sup> (short ranged RVB) with short-ranged bonds and gapped spinons will be our concern in this paper. A post-cuprate version with longer-ranged bonds and gapless spinons<sup>5</sup> has also been the subject of recent progress.<sup>6</sup> Readers familiar with one dimensional lore will note that the short-ranged and long-ranged RVBs generalize the physics, respectively, of the Majumdar-Ghosh chain<sup>7</sup> and the Bethe chain<sup>8</sup> to higher dimensions.

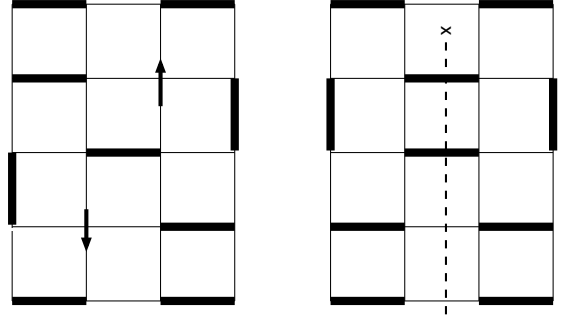


FIG. 2: Typical excitations of an RVB liquid. The left figure depicts a pair of *spinons*, fractionalized excitations with  $S = 1/2$ , formed by breaking a valence bond. Spinons are unpaired spins which move in the RVB liquid background; the interaction between spinons depends on the lattice geometry. The right figure depicts a *vison*, which is an excitation within the valence bond subspace. If we consider an RVB liquid which is an equal amplitude superposition of nearest-neighbor valence bond states, then the vison is defined by the wavefunction  $|\psi_v\rangle = \sum_c (-1)^{N_c} |c\rangle$  where  $N_c$  is the number of bonds which cross the dashed line shown in the figure. Clearly this state is orthogonal to the RVB state,  $|\psi\rangle = \sum_c |c\rangle$ . The interaction between spinons and visons is discussed in detail in Ref. 3.

The important progress that we have described has been kinematical. It has not directly answered the question of realizing RVB phases for actual Hamiltonians. The original proposal was made for the nearest-neighbor Heisenberg model on the triangular lattice but that is now generally believed to exhibit weak Néel order<sup>9</sup>. To make progress on the dynamical front, Rokhsar and Kivelson<sup>10</sup> introduced the quantum dimer model (QDM) which assumes that the low energy dynamics is dominated by valence bond configurations of short range which are taken to be nearest-neighbor in the versions studied to date. Such configurations are labelled by dimer coverings of the lattice at issue and the quantum dimer Hamiltonian acts in a Hilbert space spanned by such coverings. The program of studying the simplest dimer models has been rather fruitful. It is now clear that  $Z_2$  RVB phases may arise on non-bipartite lattices in  $d \geq 2$ <sup>11,12</sup> while bipartite lattices in  $d > 2$  give rise to  $U(1)$  RVB phases that exhibit a gapless “photon”<sup>13,14</sup>. In addition a variety of crystalline phases have been identified, most notably a Cantor deconfined region<sup>15</sup> of interleaved commensurate and incommensurate valence bond crystals on bipartite lattices in  $d = 2$ .

The next order of business then, is to find rotationally invariant, local, spin Hamiltonians that are accurately described by these well understood dimer models. This is the problem that we solve in this paper thus completing a program initiated by Chayes, Chayes and Kivelson<sup>16</sup>. The strategy we follow is that of constructing Klein Hamiltonians<sup>17</sup> with large energy scales which select nearest neighbor valence bond states as their ground states, separated by a gap from excited states. We then lift this degeneracy by the inclusion of perturbations that precisely mimic the terms in the quantum dimer models of interest. To control this procedure, with its difficulties stemming from the non-orthogonality of the valence bond basis, we introduce a parameter which is the extent of decoration of the reference lattice. By suitably tuning this parameter we are able to make our dimer model realizations arbitrarily accurate. An elegant feature of this limit is that it enables us to establish the existence of a gap about the nearest-neighbor valence bond manifold and to discuss the states above this gap in terms of “microscopic” spinons whose meaning will become clear below.

We note that our tuning procedure occurs within the space of  $SU(2)$  invariant Hamiltonians. This is in contrast to approaches involving enlarging the symmetry group to  $Sp(N)$  or  $SU(N)$  and studying the large  $N$  limit<sup>18</sup>; in these cases, the applicability of results to  $Sp(1) \equiv SU(2)$  is not obvious.

This is also a good place to note that there is a considerable body of work on variational<sup>19</sup> and finite-size studies of some of the two-dimensional phases discussed in this paper, e.g. the early finite-size study of a multiple-spin Hamiltonian on the triangular lattice that adduced evidence for a topologically ordered phase.<sup>20</sup> A comprehensive review of such work is given in Ref. 21. This

work is complementary to ours as it deals with somewhat simpler Hamiltonians but is unable to access the thermodynamic limit in a controlled fashion. We also note that, there is a large and growing literature on more general models with topological phases which we skip in our focus on  $S = 1/2$  spin systems; this work also finds inspiration from the proposal that a quantum computer may be robustly created from a topological phase.<sup>22</sup> Finally, we note that there are encouraging reports of spin liquids in experimental systems.<sup>23,24</sup>

In the rest of the paper we give details of our constructions. We begin with a quick review of quantum dimer models and the known results on their phase diagrams in Section II. In Section III we explain our strategy with the honeycomb lattice serving as an example; this realizes the physics of bipartite dimer models in  $d = 2$ . In Section IV we show how the physics of non-bipartite dimer models in  $d = 2$  and bipartite and non-bipartite dimer models in  $d > 2$  may be obtained from spin models. In Section V we discuss two spin models on the non-bipartite pyrochlore lattice, one exhibiting a  $Z_2$  RVB phase and the other a  $U(1)$  RVB phase. We conclude with a summary (Section VI) and a set of appendices that contain some technical material.

## II. QUANTUM DIMER MODELS

For a system of spins  $\vec{s}_i$  on a lattice  $\Lambda$ , a (*nearest-neighbor*) *valence bond state* is a product wavefunction of the form  $\Psi = \prod_{\langle ij \rangle} \psi_{ij}$  where  $\psi_{ij} = \frac{1}{\sqrt{2}}(\psi_i^\uparrow \psi_j^\downarrow - \psi_i^\downarrow \psi_j^\uparrow)$  and the product is over nearest-neighbor pairs  $(i, j)$ . The product is defined so each spin forms a singlet with exactly one of its neighbors. Each valence bond state corresponds to a hard-core dimer covering of  $\Lambda$  where a dimer connecting two sites corresponds to a singlet bond between the respective spins. Valence bond states are not orthogonal but the overlap between two arbitrary states is exponentially small in the length of closed loops obtained by superposing them. This suggests that they are linearly independent on sufficiently open lattices and indeed there are proofs for many<sup>16</sup> and numerical evidence that this is so even on the triangular lattice<sup>25</sup>.

The identification with dimer coverings suggests that any low energy dynamics restricted to the valence bond manifold can be represented by a quantum dimer Hamiltonian acting on orthogonal dimer states. The simplest such Hamiltonian on the square lattice, written down by Rokhsar and Kivelson<sup>10</sup>, has the pictorial form

$$H_{\text{QDM}} = \sum -t(|\uparrow\downarrow\rangle\langle\downarrow\uparrow| + \text{h.c.}) + v(|\uparrow\downarrow\rangle\langle\uparrow\downarrow| + |\downarrow\uparrow\rangle\langle\downarrow\uparrow|) \quad (2.1)$$

where  $t$  and  $v$  are positive constants and the sum is over all possible square plaquettes. Evidently, this can be supplemented by kinetic energy terms which act on longer loops and potential energy terms which count more complicated dimer motifs.<sup>26</sup>

The passage from valence bonds to dimers, however, has to contend with two complications. One is that one needs to choose a phase convention for the valence bonds, which is subject to restrictions on what signs one can obtain for various couplings in the dimer Hilbert space. The other, already alluded to, is the lack of orthogonality of the valence bond states which makes the transcription from a spin model to a dimer model non-trivial. We will deal with both problems later in the paper; here we merely wish to alert the reader to their existence.

An important property of the quantum dimer Hamiltonian is the existence of the “Rokhsar-Kivelson point” (*RK point*)  $t = v$ , where any equal amplitude superposition of all dimer coverings connected by the operation of the kinetic energy is a ground state. To see this, note that for every flippable plaquette, the second term gives a penalty  $v$  while the first term gives at most a benefit of  $-t$ . Nonflippable plaquettes are destroyed by  $H_{QDM}$ . This gives a lower bound for the ground state energy:  $E_0 \geq \min\{0, N_P(v - t)\}$ , where  $N_P$  is the number of plaquettes in the lattice. The equal amplitude state has energy  $\langle n_{fl} \rangle(v - t)$ , where  $\langle n_{fl} \rangle$  is the average number of flippable plaquettes in the state. At  $v = t$ , this saturates the lower bound and, since the equal amplitude state is an eigenstate of  $H_{QDM}$  (at  $v = t$ ), we may conclude that it is the ground state when  $v = t$ .

Thus the ground state correlations at the RK point reduce to those of solvable classical dimer models. Additionally, the infinite temperature static correlations of QDMs also reduce to those of the same classical models. These features, along with the additional one that Hamiltonians of the form (2.1) can be simulated by Monte-Carlo without any sign problems, have been crucial to making progress in determining the phase diagrams of the quantum models.

As a consequence of this progress we now know that:

- i) QDMs on bipartite lattices in  $d = 2$  do not exhibit an RVB phase. The equal amplitude state present at the RK point,  $v/t = 1$ , does not extend into a phase. As  $v/t$  increases, the system generically passes through a sequence of interleaved commensurate and incommensurate crystalline phases before reaching the staggered valence bond solid (VBS) phase. These intermediate phases, whose measure approaches unity near the RK point, turn out to have deconfined monomers, a phenomenon coined Cantor deconfinement<sup>15</sup>. As  $v/t$  decreases from unity, the system passes through a plaquette phase<sup>27</sup> before undergoing a first-order transition to a columnar VBS.
- ii) QDMs on non-bipartite lattices in  $d = 2$  may exhibit RVB phases. These are  $Z_2$  RVB phases captured by a purely topological  $BF$  theory<sup>3</sup>. For the triangular lattice, it has been shown<sup>11</sup> that for  $v/t > 1$ , the system is in a staggered VBS; for  $v/t \leq 1$ , there is a deconfined RVB liquid phase. As  $v/t$  is further reduced, there are probably a small number of VBS phases culminating in the columnar state.
- iii) QDMs on non-bipartite lattices in  $d = 3$  and higher

also exhibit a  $Z_2$  RVB phase<sup>12</sup>.

- iv) QDMs on bipartite lattices in  $d = 3$  and higher exhibit a  $U(1)$  RVB phase with a gapless, linearly dispersing transverse mode, the “photon”<sup>13</sup>.

We now turn to the task of constructing spin models whose low energy dynamics is precisely captured by these dimer models. We begin, for pedagogical specificity, with the honeycomb lattice.

### III. HONEYCOMB LATTICE: BIPARTITE PHYSICS IN $d = 2$

Our strategy for realizing dimer models proceeds in three steps. First, we construct, following Klein, a local spin Hamiltonian that has valence bond states as its ground states. Next we perturb it to obtain a QDM. Finally, we decorate the lattice to simplify the QDM to the well studied form (2.1). In the high decoration limit, we show the existence of a gap and give a description of the spectrum in terms of spinons.

#### A. Klein model

The basic idea of the Klein model consists of considering a cluster of  $z$  sites (typically, a spin and its  $z-1$  neighbors) and deterring, via an energy penalty, this cluster from having maximal total spin  $S_{tot} = z/2$ . If two of the spins in the cluster form a singlet bond, this condition is satisfied. This is why Klein Hamiltonians naturally lead to valence bond ground states.

In particular, for a system of spins  $\vec{s}_i$  on a lattice  $\Lambda$ , a Klein Hamiltonian is a sum of projection operators  $\hat{P}_{\mathcal{N}(i)}$  defined as follows. For each site  $i$ , consider the neighborhood of spins  $\mathcal{N}(i)$  consisting of the spin at site  $i$  and its  $(z_i - 1)$  nearest neighbors. Let  $\hat{P}_{\mathcal{N}(i)}$  be the projector onto the highest total spin state of the cluster. The Klein Hamiltonian is formally given by the expression:

$$H_K = \sum_{i \in \Lambda} \hat{P}_{\mathcal{N}(i)} , \quad (3.1)$$

with total spin of cluster  $\mathcal{N}(i)$  given by:

$$\vec{S}_{\mathcal{N}(i)} = \sum_{j \in \mathcal{N}(i)} \vec{s}_j \quad (3.2)$$

We may write  $\hat{P}_{\mathcal{N}(i)}$  in terms of this operator. For example, if  $z_i$  is even, then:

$$\hat{P}_{\mathcal{N}(i)} = C_i \prod_{L=0}^{z_i/2-1} \left[ S_{\mathcal{N}(i)}^2 - L(L+1) \right] . \quad (3.3)$$

The total spin of this cluster will take values from  $0, 1, \dots, (z_i/2) - 1, z_i/2$ . The factors of this product are operators which sequentially annihilate all but the highest

spin sector. The form of the operator implies that larger clusters involve higher-order spin interactions— but they always remain local.

If the constants  $C_i$  in Eq. 3.3 are chosen to be positive, then  $H_K$  will have non-negative eigenvalues. By construction, valence bond coverings are zero-energy ground states of  $H_K$ .

For the honeycomb lattice, Chayes *et al.*<sup>16</sup> have already written down the explicit form of the Klein Hamiltonian in terms of spin operators. Their expression, up to unimportant overall constants, is:

$$H = \sum_{\langle i,j \rangle} \vec{s}_i \cdot \vec{s}_j + \frac{1}{2} \sum_{\langle\langle i,j \rangle\rangle} \vec{s}_i \cdot \vec{s}_j + \frac{2}{5} \sum'_{ijkl} (\vec{s}_i \cdot \vec{s}_j)(\vec{s}_k \cdot \vec{s}_r) \quad (3.4)$$

The first and second terms are over nearest and next nearest neighbors respectively. The third term is over quartets  $ijkl$  where  $i$  and  $j$  are nearest neighbors;  $k$  is a neighbor of  $i$  different from  $j$ ; and  $r$  is a neighbor of  $j$  different from  $i$ . A striking feature of this Hamiltonian is that the leading term is the usual Heisenberg antiferromagnet.

### B. Perturbations

We will now perturb the Klein Hamiltonian to obtain a QDM with dynamics. In doing so we will use the *overlap expansion* invented by Rokhsar and Kivelson<sup>10</sup>, which is predicated on the linear independence of the valence bond states. That valence bond states on the honeycomb lattice are linearly independent was proved in Ref. 16.

For the purpose of obtaining the dimer kinetic energy, it is sufficient to consider including just an additional nearest neighbor interaction<sup>28</sup>,

$$\delta H = \sum_{\langle i,j \rangle} \vec{s}_i \cdot \vec{s}_j \quad (3.5)$$

To first order in degenerate perturbation theory, we may write this as an effective operator on the valence bond states. First, we define an orthonormal basis set  $\{|\alpha\rangle\}$  in terms of the linearly independent valence bond states  $\{|i\rangle\}$ :

$$|\alpha\rangle = \sum_i (S^{-1/2})_{\alpha,i} |i\rangle \quad (3.6)$$

Here  $S_{ij} = \langle i|j\rangle$  is the overlap matrix element between valence bond states  $|i\rangle$  and  $|j\rangle$ . The magnitude of the overlap of two valence bond states may be determined by overlaying the two configurations forming what is called the *transition graph*<sup>10</sup>. The construction is described in Fig. 3. As shown in Fig. 3, the transition graph consists of double bonds, where the two states have a bond in common, and closed loops of varying (even) lengths. The

magnitude of the overlap  $S_{ij}$  is given by  $2^{N_l} \prod_i x^{L_i}$  where  $N_l$  is the number of loops; the product is over all such loops;  $L_i$  is the length of loop  $i$ ; and  $x = \frac{1}{\sqrt{2}}$ . The sign of  $S_{ij}$  depends on how we choose to orient the bonds. By orientation, we refer to the fact that a bond between sites 1 and 2 may be interpreted as the singlet bond  $\psi_{12} = \frac{1}{\sqrt{2}}(\psi_1^\uparrow \psi_2^\downarrow - \psi_1^\downarrow \psi_2^\uparrow)$  or as  $\psi_{21} = -\psi_{12}$ . The key idea of the overlap expansion is to treat  $x$  as a small expansion parameter.

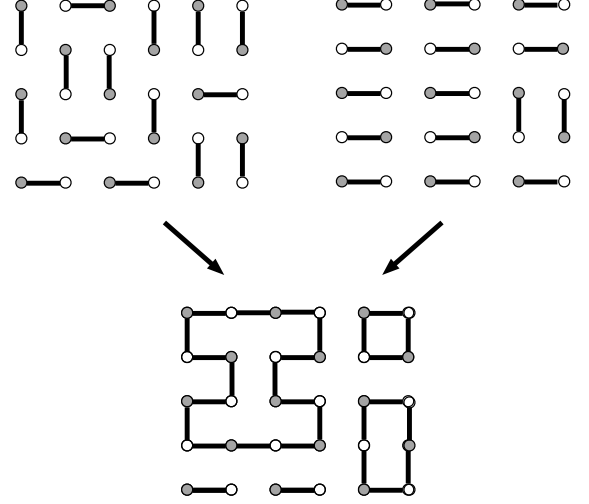


FIG. 3: Transition graph construction for two valence bond coverings of the square lattice (the construction for other lattices is similar). The dots are the lattice sites and the thick lines denote that the two sites form a singlet bond. The singlet orientation may be specified, for example, by having the bonds point from the gray sites to the white sites. The transition graph is formed by overlaying the two configurations resulting in a graph (lower) containing double bonds and closed loops of varying (even) lengths. In the above example, there are two double bonds and three loops of lengths 4, 6, and 16. The magnitude of the overlap between the two valence bond coverings is then given by  $|S| = 2^3 (1/\sqrt{2})^{4+6+16} = (\frac{1}{2})^{10} = \frac{1}{1024}$ . Thus, while the overlap between two arbitrary valence bond coverings is never zero, it is usually a small number. This is the basis for the overlap expansion discussed in the text.

We may specify the matrix elements of our effective operator in terms of the  $\{|\alpha\rangle\}$  basis:

$$H_{\alpha\beta} = (S^{-1/2} \delta H S^{-1/2})_{\alpha\beta} \quad (3.7)$$

$$= \sum_{ij} (S^{-1/2})_{\alpha,i} \langle i | \delta H | j \rangle (S^{-1/2})_{j,\beta} \quad (3.8)$$

If either state  $|i\rangle$  or  $|j\rangle$  contains the bond  $(12)$ , then  $\langle i | \vec{s}_1 \cdot \vec{s}_2 | j \rangle = -\frac{3}{4} \langle i | j \rangle$ . If neither  $|i\rangle$  nor  $|j\rangle$  contains the bond  $(12)$ , then we have a non-zero matrix element only if spins 1 and 2 are members of the same loop in the transition graph. If that is the case, then one may show that  $\langle i | \vec{s}_1 \cdot \vec{s}_2 | j \rangle = (-1)^{n/2} (\mp \frac{3}{4}) \langle i | j \rangle$  where  $n$  is the length of the

loop for the case where spins 1 and 2 are separated by an even (odd) number of sites.

We now specialize to the honeycomb lattice. As sketched in the Appendix, we may orient the bonds on the honeycomb lattice so that for any two states differing by a (minimal) length 6 loop, the overlap  $\langle i|j \rangle$  has a positive sign. On the honeycomb lattice, the sign is a matter of convention and we could have chosen the negative sign. Given the positive sign convention, we conclude that our matrix element is given by:

$$\langle i|\delta H|j \rangle = -\frac{3n_d}{4}\delta_{ij} - \frac{3}{4}(2x^6)\odot_{ij} + O(x^{10}) \quad (3.9)$$

where  $n_d$  is the number of bonds (half the number of sites) and  $\odot_{ij}$  is a matrix that is 1 if states  $|i \rangle$  and  $|j \rangle$  differ by a length 6 loop and zero otherwise. We may also expand the overlap matrix:

$$S_{ij} = \delta_{ij} + 2x^6\odot_{ij} + O(x^{10}) \quad (3.10)$$

$$(S^{-1/2})_{ij} = \delta_{ij} - x^6\odot_{ij} + O(x^8) \quad (3.11)$$

Comparing the previous line with Eq. 3.6, we see that within the overlap expansion, each  $|\alpha \rangle$  has a largest component corresponding to a unique valence bond state. Therefore, we will refer to the orthogonal set  $\{|\alpha \rangle\}$  as the set of *dimer* states corresponding to the valence bond coverings. In writing our effective operator, we absorb the leading term involving the number of dimers  $n_d$  times the unit operator into our definition of zero energy.

$$\begin{aligned} H_{\alpha\beta} &= \sum_{ij} [\delta_{\alpha i} - x^6\odot_{\alpha i} + O(x^8)] \\ &\times [-\frac{3}{4}(2x^6)\odot_{ij} + O(x^{10})] \\ &\times [\delta_{j\beta} - x^6\odot_{j\beta} + O(x^8)] \\ &\approx -\frac{3}{4}(2x^6)\odot_{\alpha\beta} + O(x^{10}) \end{aligned} \quad (3.12)$$

$$(3.13)$$

We conclude that the leading term in the overlap expansion is an operator with nonzero matrix elements only between dimer states differing by a minimal length 6 loop. All of these nonzero elements have the same value  $-t = -(3/4)(2x^6)$ . Thus we have obtained the kinetic energy operator in the quantum dimer model (QDM). Note that we can conclude this only because we were able to define a bond orientation convention such that all minimal overlaps come with the same sign. Otherwise some off-diagonal terms would have energy  $t$  and the energy bound arguments which we gave previously to conclude that there is an RVB state at the RK point would no longer hold.

To obtain the potential energy term as the leading order effect, we need a more complicated interaction which we take to be:

$$\delta H = J \sum_{\langle ij \rangle} \vec{s}_i \cdot \vec{s}_j +$$

$$\begin{aligned} &v \sum_{\odot} \left( (\vec{s}_1 \cdot \vec{s}_2)(\vec{s}_3 \cdot \vec{s}_4)(\vec{s}_5 \cdot \vec{s}_6) \right. \\ &\left. + (\vec{s}_2 \cdot \vec{s}_3)(\vec{s}_4 \cdot \vec{s}_5)(\vec{s}_6 \cdot \vec{s}_1) \right) \end{aligned} \quad (3.14)$$

where the first sum is over nearest neighbors and the second sum is over elementary plaquettes (see Fig. 4).

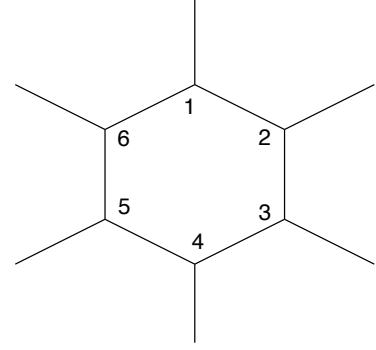


FIG. 4: The elementary plaquette of the honeycomb lattice.

The first term of Eq. 3.14 gives the QDM kinetic energy. Similarly, consider the operator  $s_{12}s_{34}s_{56} = (\vec{s}_1 \cdot \vec{s}_2)(\vec{s}_3 \cdot \vec{s}_4)(\vec{s}_5 \cdot \vec{s}_6)$ . If valence bond states  $|i \rangle$  and  $|j \rangle$  contain the bonds (12), (34), and (56), then  $\langle i|s_{12}s_{34}s_{56}|j \rangle = (-\frac{3}{4})^3 \langle i|j \rangle$ . If state  $|i \rangle$  contains all three bonds, then the diagonal matrix element  $\langle i|s_{12}s_{34}s_{56}|i \rangle$  is  $(-\frac{3}{4})^3$ . If state  $|i \rangle$  is missing one or more bonds, then the diagonal matrix element is zero unless  $|i \rangle$  contains the three complementary bonds (23), (45), and (61). In this case, the expectation of the operator equals  $(-\frac{3}{4})^3 x^6$ , which is higher order in the overlap expansion. It may be shown that off-diagonal matrix elements evaluate to a term proportional to the overlap of the states, the proportionality constant being of order unity. These results imply that the matrix element of the ring interaction between two valence bond states is given by:

$$\left(-\frac{3}{4}\right)^3 v n_{fl,i} \delta_{ij} + O(vx^6) \quad (3.15)$$

where  $n_{fl,i}$  is the number of flippable hexagonal plaquettes in configuration  $|i \rangle$ . We may write this in terms of dimer states, as discussed above. Absorbing numerical factors into the constants  $J$  and  $v$ , we arrive at our effective dimer Hamiltonian:

$$\begin{aligned} H_{\alpha\beta} &= -Jx^6\odot_{\alpha\beta} + v n_{fl,\alpha} \delta_{\alpha\beta} + O(vx^6 + Jx^{10}) \\ &= -t\odot_{\alpha\beta} + v n_{fl,\alpha} \delta_{\alpha\beta} + O(vx^6 + tx^4) \end{aligned} \quad (3.16)$$

where  $t = Jx^6$  and  $n_{fl,\alpha}$  is the number of flippable plaquettes in the valence bond state corresponding to dimer state  $\alpha$ . If  $t$  and  $v$  are of order unity, then the higher order terms will be small compared to the first two terms, which act on our dimer states (which are really spin states) in a manner analogous to the QDM kinetic and potential energy operators on usual dimer states.

For the actual problem at hand,  $x = (1/\sqrt{2})$  is less than 1 but is by no means tiny. Hence the neglect of other terms induced by our perturbations is not obviously justified. While we do not need them to be zero, we do need them to be weak enough perturbations so the analysis of Ref. 10 is justified.

What we do learn from the overlap expansion result (3.16) is that the non-orthogonality is a much smaller problem on more open lattices which involve large loops. While the honeycomb is a good candidate on this score, to put the issue beyond doubt we now consider a decorated version of the lattice.

### C. Decoration scheme

In this section, we propose a modification to our earlier arguments which makes the overlap expansion essentially exact. Consider the decorated honeycomb lattice shown in Fig. 5 where we insert  $N$  (an even integer) sites between neighboring sites of the usual honeycomb lattice. The dimer structure of this lattice, including the number of dimer states, is exactly the same as before except that having a dimer between sites 1 and 2 corresponds to a chain of  $(N+2)/2$  dimers beginning at site 1 and ending at site 2. Not having a dimer between sites 1 and 2 corresponds to having a chain of  $N/2$  dimers beginning at site  $b_1$  and ending at site  $a_2$ . The Klein Hamiltonian is correspondingly modified by including Klein projectors for the added sites.

Majumdar and Ghosh<sup>7</sup> showed that the valence bond state is the only ground state of the Klein Hamiltonian for a one-dimensional spin chain with an even number of spins. Therefore, the conclusions regarding the Klein model on the honeycomb lattice (linear independence of valence bond states, valence bond states span the ground state manifold, etc) carry over directly to the decorated honeycomb lattice.

While decorating does not introduce any new technical problems, there is a significant technical advantage with respect to the overlap expansion. The smallest two loops on the hexagonal lattice are length 6 and 10 from which we obtained that the relative orders of the leading and error terms in the overlap expansion were  $x^6$  and  $x^{10}$ . The smallest loops on the decorated hexagonal lattice have lengths  $6(N+1)$  and  $10(N+1)$ . Repeating the previous analysis, we will find that the leading and error terms in the overlap expansion are  $x^{6(N+1)}$  and  $x^{10(N+1)}$ . The ratio of error term to leading term has improved from  $x^4$  to  $x^{4N}$ . In the large  $N$  limit, the error term is “rigorously” negligible but we propose that even fairly small values of  $N$  may suffice to capture the qualitative features of the large  $N$  limit.

While we have added complexity to the lattice, we do not have to increase the order of the spin interaction. Consider the following as a perturbation to the decorated

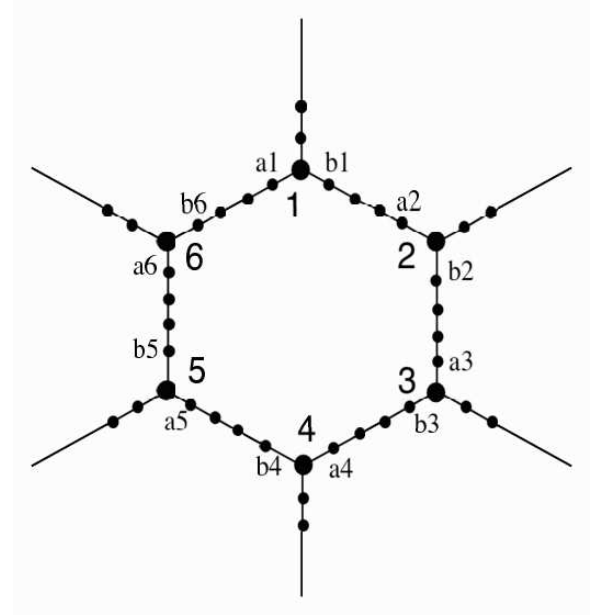


FIG. 5: The decorated honeycomb lattice where  $N$  (an even integer) two-fold sites are inserted between the old sites. This drawing shows  $N = 4$ . The labels  $a_1$  and  $b_1$  designate the first counterclockwise and first clockwise neighbor of spin 1 where clockwise is with respect to the loop 123456. For the undecorated case,  $a_1$  and  $b_1$  are just sites 6 and 2.

honeycomb lattice Klein model:

$$\begin{aligned} \delta H = & J \sum_{\langle ij \rangle} \vec{s}_i \cdot \vec{s}_j + \\ & v \sum_{\square} \left( (\vec{s}_1 \cdot \vec{s}_{b_1})(\vec{s}_3 \cdot \vec{s}_{b_3})(\vec{s}_5 \cdot \vec{s}_{b_5}) \right. \\ & \left. + (\vec{s}_1 \cdot \vec{s}_{a_1})(\vec{s}_3 \cdot \vec{s}_{a_3})(\vec{s}_5 \cdot \vec{s}_{a_5}) \right) \end{aligned} \quad (3.17)$$

The first term is a nearest neighbor interaction over all spins while the second term is over all elementary plaquettes, such as the one in Fig. 5. A 6 spin interaction is sufficient, even though we have many more spins in the loop, because having a  $(1b_1)$  bond automatically implies the other bonds in the chain connecting 1 and 2. Our previous analysis carries over to the present case and we conclude:

$$\begin{aligned} H_{\alpha\beta} = & -Jx^{6(N+1)}\square_{\alpha\beta} + vn_{fl,\alpha}\delta_{\alpha\beta} \\ & + O(vx^{6(N+1)} + Jx^{10(N+1)}) \\ = & -t\square_{\alpha\beta} + vn_{fl,\alpha}\delta_{\alpha\beta} + O(vx^{6(N+1)} + tx^{4N}) \end{aligned} \quad (3.18)$$

where  $t = Jx^{6(N+1)}$  and otherwise the notation is the same.

Clearly, by decorating enough we can make the matrix elements beyond the dimer model arbitrarily small and thus realize the physics, including Cantor deconfinement,

present in generic, weak perturbations of the honeycomb QDM.

### 1. Spinons

In the highly decorated limit, one may show that nearest-neighbor valence bond states are separated by a finite gap from the excited states of the Klein model. In this limit, we are connecting a set of Majumdar-Ghosh<sup>7</sup> (MG) chains into a two-dimensional network. We may describe the excited states of our system in terms of the well studied spinon defects of the MG chains, which are widely believed to be gapped<sup>29,30,31</sup>. Here we give an outline of our argument and relegate technical details to Appendix B.

In Appendix B, we consider what happens when we put these chains together for different values of a tunable parameter in our model: the ratio of Klein scales (the coefficient  $C_i$  in Eq. 3.3) of the Klein projectors of the decorated and reference sites. For large values of this ratio, the excited states are represented by “microscopic” spinons localized on the reference sites. For small values of the Klein ratio, the excited states are extended and may be interpreted as MG spinons scattering at the vertices. There is a first order transition between these limits. In both limits, there is a gap between the VB manifold and the spinon states, as depicted in Fig. 6.

Spinons are the natural excited states (outside of the VB manifold) in the high decoration limit. For an unperturbed Klein model, the VB manifold is degenerate so these excitations are mobile. The next question is what happens when the degeneracy of the ground state manifold is lifted. We argue that this has a small but vital effect on the spinon dynamics. At the RK point and in liquid phases, we expect the spinons to be deconfined. In the crystalline phases, we may consider a pair of test spinons, holding one member fixed and considering the quantum mechanics of the other. If the wavefunction of the non-fixed spinon has spatial extent  $L$ , this would have an energy cost of order  $\epsilon_c L^2$  where  $\epsilon_c$  is the energy cost per unit area of scrambling the crystalline background. The  $L$ -dependence of the kinetic energy varies as  $1/L^2$ . The implication is that while  $\epsilon_c$  is a much smaller scale than the spinon gap, spinons moving in a crystalline background are confined at sufficiently long length scales.

### D. Square lattice

The square lattice is another two-dimensional bipartite lattice for which (nearest-neighbor) valence bond states are linearly independent<sup>16</sup>. We may orient the bonds on the square lattice so that two states differing by a (minimal) length 4 loop, have positive overlap. The problem with applying our approach to the bare square lattice is that the Klein model has ground states outside of the valence bond manifold (Fig. 7). These extra states do not

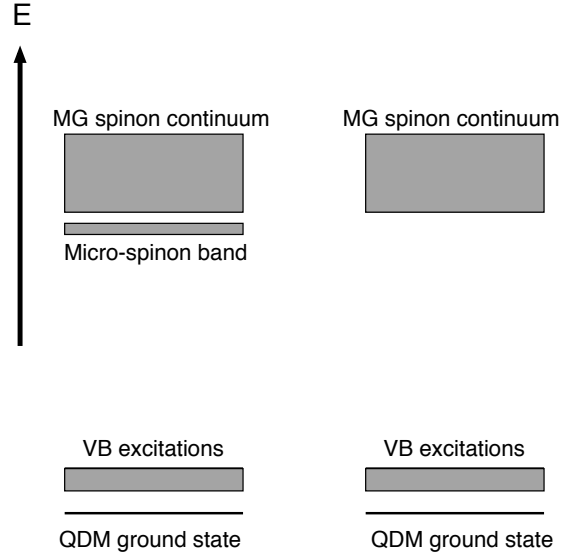


FIG. 6: A cartoon of the spectra for the limiting cases where the Klein ratio is large (left) and small (right). In the small Klein ratio case (right), the lowest excited states are described by extended spinon wavefunctions. These scattering states are present even in the large ratio case (left) but here the lowest excitations, which we call “microscopic” spinons, are described by a wavefunction having peaks at the reference sites and decaying on the chains. The decay rate can be made arbitrarily fast by tuning the Klein ratio. The bandwidth of these localized states depends on the decoration and is zero in the infinite decoration limit. Details are given in Appendix B.

arise when we consider the decorated square lattice. Consider perturbing a decorated square lattice Klein model with:

$$\delta H = J \sum_{\langle ij \rangle} \vec{s}_i \cdot \vec{s}_j + v \sum_{\square} \left( (\vec{s}_1 \cdot \vec{s}_{b_1})(\vec{s}_3 \cdot \vec{s}_{b_3}) + (\vec{s}_1 \cdot \vec{s}_{a_1})(\vec{s}_3 \cdot \vec{s}_{a_3}) \right) \quad (3.19)$$

where the first term is a nearest neighbor interaction and the second sum is over all elementary plaquettes, the spins 1234 labelling the 4 sites of a square plaquette in clockwise order and, as before (see Fig. 5), the labels  $a_i$  and  $b_i$  denoting the first counterclockwise and first clockwise neighbor of spin  $i$ . By arguments similar to the honeycomb case, we obtain an effective Hamiltonian:

$$\begin{aligned} H_{\alpha\beta} &= -Jx^{4(N+1)}\square_{\alpha\beta} + vn_{fl,\alpha}\delta_{\alpha\beta} \\ &+ O(vx^{4(N+1)} + Jx^{6(N+1)}) \\ &= -t\square_{\alpha\beta} + vn_{fl,\alpha}\delta_{\alpha\beta} + O(vx^{4(N+1)} + tx^{2N}) \end{aligned} \quad (3.20)$$

Here  $\square_{ij}$  is a matrix that is 1 if states  $|i\rangle$  and  $|j\rangle$  differ by the (minimal) length 4 loop and zero otherwise. There-

fore, we realize the physics of the square lattice QDM. Note that without the decoration, the error would be order  $x^2 = (1/2)$ , as opposed to the bare honeycomb case where the error is order  $x^4 = (1/4)$ .

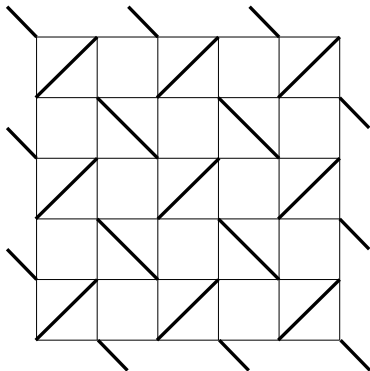


FIG. 7: The Klein model for the square lattice, with periodic boundary conditions, permits ground states which are not in manifold spanned by nearest-neighbor valence bond states such as this one. Here the thin lines form the lattice and the thick lines denote singlet pairings. Note that the Klein condition is satisfied at every lattice site.

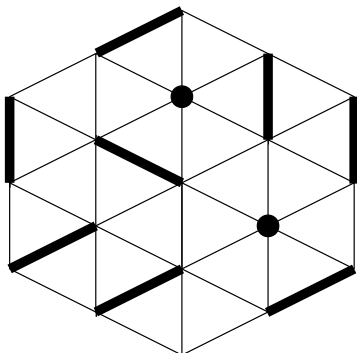


FIG. 8: The Klein model for the triangular lattice admits many nontrivial non-dimer ground states, such as this one. The thin lines show the lattice and the thick lines denote singlet pairings. The dots represent free spins. Note that the Klein condition is satisfied at every lattice site.

#### IV. OTHER VALENCE BOND PHASES IN $d = 2$ AND $d = 3$

We now sketch the application of our strategy to obtain the rest of dimer model physics, including RVB phases. The points to be made concern the choice of lattices and phase conventions.

##### A. Non-bipartite lattices in $d = 2$

The simplest  $d = 2$  non-bipartite lattice is the triangular lattice. Numerical evidence suggests that (nearest-neighbor) valence bond states are linearly independent.<sup>25</sup> As with the square and honeycomb lattices, we may orient bonds so that states differing by a (minimal) length 4 loop, have positive overlap.<sup>32</sup> As with the square lattice, the Klein model admits non-valence bond ground states, though the problem is more serious with the triangular lattice (see Fig. 8). Decoration eliminates these possibilities by removing the triangular nearest-neighbor structures. Applying our strategy to the decorated triangular lattice allows us to reproduce the physics of the triangular lattice QDM, including its RVB phase<sup>11</sup>. By calculations similar to Appendix B, one may show that spinon excitations are gapped. For the triangular lattice, it is known that collective excitations within the valence bond manifold are also gapped<sup>11,33</sup>, a conclusion which will remain valid for the decorated case. Therefore, we have constructed a model that shows a stable,  $SU(2)$ -invariant RVB liquid phase.

Another non-bipartite lattice is the pentagonal lattice<sup>34</sup> shown in Fig. 9. There are currently no formal proofs for the pentagonal lattice regarding the issues of linear independence of (nearest-neighbor) valence bond states and whether the set of these states spans the ground state space of the corresponding Klein model. However, it was explained in Ref. 16 that the most important ingredients of their proofs for the honeycomb lattice are its relatively low coordination number (3); relatively large minimum loop size (6); and the absence of triangular structures in the lattice. The pentagonal lattice, has sites of coordination 3 and 4, minimum loop size 8, and no triangular structures, suggesting that the arguments may be adapted to this lattice. As before, it is possible to orient bonds so that the overlap of states differing by a (minimal) length 8 loop always has the same sign. While in the square, triangle, and honeycomb cases, the sign of the overlap is a matter of convention (which we chose as positive), for the pentagonal lattice, only the negative sign is possible. In fact, in Appendix A, it is shown that using the fermionic convention, one may always obtain the negative sign independent of lattice details. Therefore, to generate the QDM kinetic energy, we must perturb the Klein model with a ferromagnetic interaction. From a perturbation of the form:

$$\begin{aligned} \delta H = & -J \sum_{\langle ij \rangle} \vec{s}_i \cdot \vec{s}_j + \\ & v \sum_{\bigcirc} \left( (\vec{s}_1 \cdot \vec{s}_{b_1})(\vec{s}_3 \cdot \vec{s}_{b_3})(\vec{s}_5 \cdot \vec{s}_{b_5})(\vec{s}_7 \cdot \vec{s}_{b_7}) \right. \\ & \left. + (\vec{s}_1 \cdot \vec{s}_{a_1})(\vec{s}_3 \cdot \vec{s}_{a_3})(\vec{s}_5 \cdot \vec{s}_{a_5})(\vec{s}_7 \cdot \vec{s}_{a_7}) \right) \quad (4.1) \end{aligned}$$

where the first term is over all nearest-neighbor spins and the second term is over elementary plaquettes ( $a_i$  and  $b_i$ , once again, denoting the first counterclockwise



and first clockwise neighbors of spin  $i$ ), we may obtain the quantum dimer Hamiltonian for the decorated pentagonal lattice:

$$H_{\alpha\beta} = -t\bigcirc_{\alpha\beta} + v n_{fl,\alpha} \delta_{\alpha\beta} + O(vx^{8(N+1)} + tx^{2N}) \quad (4.2)$$

Here  $\bigcirc_{ij}$  is a matrix that is 1 if states  $|i\rangle$  and  $|j\rangle$  differ by the (minimal) length 8 loop and zero otherwise. Therefore, we realize the physics of the pentagonal lattice QDM. We have checked that in the classical limit, the dimer-dimer correlations decay exponentially and in Appendix C, we present numerical evidence that monomers are deconfined. As both features also hold at the RK point, we may repeat the arguments described in Ref. 11 for the triangular lattice to conclude that the pentagonal lattice QDM also shows an RVB liquid phase, a result which may be transcribed into spin language as discussed above.

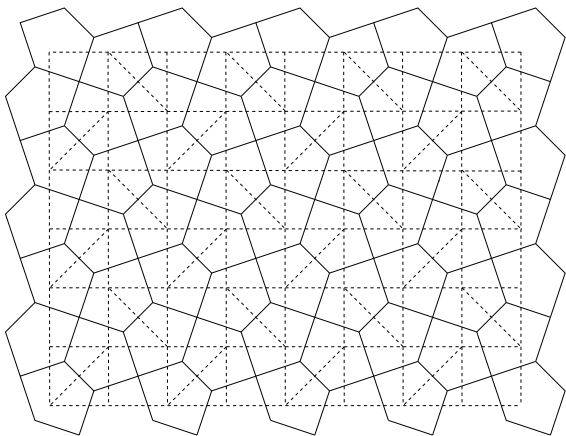


FIG. 9: The pentagonal (Sutherland-Shastry) lattice. It is the dual of the Shastry-Sutherland lattice, which is indicated by the dashed lines.

### B. Non-bipartite lattices in $d = 3$

The face-centered cubic (FCC) is a three-dimensional non-bipartite Bravais lattice with each site having 12 nearest-neighbors. The undecorated lattice has triangular structures involving two neighboring facial sites and the two corners which are their common neighbors. This will lead to non-valence bond ground states in the FCC Klein model. Decoration eliminates the triangular structure and hence this type of pathology. The shortest resonance loops are length 4. In the fermion sign convention, these loops come with negative sign. A perturbation consisting of a ferromagnetic exchange and 4-spin resonance interaction will reproduce the QDM results for the decorated lattice. We expect the resulting model to show a  $Z_2$  RVB phase near its RK point<sup>12</sup>.

### C. Bipartite lattices in $d = 3$

For the diamond lattice we pursue the same strategy as above. The properties of the diamond lattice we require are the following.

The diamond lattice is bipartite, has coordination four, and the shortest resonance loops are of length six. The Klein Hamiltonian again has nearest-neighbour dimer coverings as ground states, although, as for the case of the pentagonal lattice, no theorem exists excluding other ground states. It is likely that extra states may be excluded by decorating the lattice. The number of dimer ground states,  $n_{gs}$ , is exponentially large in the number of sites,  $N$ , but it is not known exactly. Defining the ground state entropy per site as  $\mathcal{S} = (1/N) \ln n_{gs}$ , an accurate series expansion by Nagle<sup>35</sup> yields  $\mathcal{S} \approx 0.265$ .

We now try to mimic an RK quantum dimer model for the diamond lattice. As for the case of the honeycomb lattice, we do this by adding a nearest-neighbour exchange term to induce a kinetic term and in addition, a ring term to generate a potential term. We then expect the resulting model to exhibit, near the effective RK point, a  $U(1)$  RVB liquid phase with algebraically decaying correlations as well as gapless photonic gauge excitations, as discussed in detail in Ref. 13.

This liquid phase will give way, upon making the potential term more attractive, to a columnar-type solid. For an increasingly repulsive potential, the scenario of Cantor deconfinement predicted for the two-dimensional case is simplified. Technically, there are no relevant lock-in terms in three dimensions so that the deconfined region simply acquires an increasing amount of  $U(1)$  flux as  $v/t$  is increased through the RK point; finally, a staggered solid, with the maximal amount of  $U(1)$  flux allowed by microscopic constraints,<sup>12,13,15</sup> is reached. We cannot say whether this will happen continuously or via a first order transition.

## V. DYNAMICAL SELECTION OF GAUGE STRUCTURES: PYROCHLORE LATTICE

We construct a Klein model with  $Z_2$  order and a Kivelson-Klein model with  $U(1)$  order which takes advantage of the bipartiteness of the dual lattice. This nicely illustrates the dynamical selection of the low-energy gauge structure present in topological phases.

### A. The Klein model

The undecorated pyrochlore lattice (Fig. 10) does not lend itself straightforwardly as a starting point for dimer models obtained via the Klein route because its basic building block, the tetrahedron, supports more dimer coverings than linearly independent singlet states. By sufficiently decorating the lattice, the orthogonality problem is solved. The shortest resonance loops are length 6

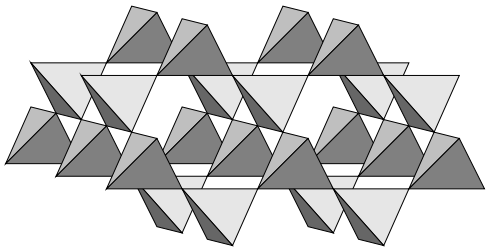


FIG. 10: The pyrochlore lattice, a network of corner-sharing tetrahedra

and the fermionic convention may be used to make the minimal overlaps come with negative sign. Perturbing the decorated pyrochlore Klein model with a ferromagnetic nearest-neighbor interaction and 6-spin ring interaction, we obtain an effective Hamiltonian mimicking the pyrochlore lattice QDM, which includes a  $Z_2$  RVB phase.

### B. The Kivelson-Klein model

A modified version of the Klein Hamiltonian, which we will refer to as the Kivelson-Klein Hamiltonian, may be used to produce a model displaying a  $U(1)$  RVB phase.<sup>36</sup> Its Hamiltonian is of the same form as Eq. 3.1 but the definition of  $\mathcal{N}(i)$  is changed. The projection now acts not on a site and its nearest neighbours but instead on the four sites of a tetrahedron:

$$H_{KK} = \sum_{tet} \hat{P}_{tet}. \quad (5.1)$$

We note that the simple decoration trick described above cannot as usefully be applied to the Kivelson-Klein model, as here increasing the number of sites in the tetrahedron does not lead to an increase in the number of dimers required.

#### 1. Ground states of the Kivelson-Klein model

Evidently, each state in which each tetrahedron contains at least one singlet bond is a ground state of the above Hamiltonian, Eq. 5.1. How can this be related to dimer coverings of the pyrochlore lattice?

First, note that (i) the number of tetrahedra equals twice the number of sites,  $N_t = 2N$ , and that (ii) the number of hardcore dimers,  $N_d \leq N/2$ , as a dimer involves two sites. From this it follows that  $N_d \leq N_t$ , the equality sign holding for hardcore dimer *coverings*. However, the requirement of having at least one dimer in *each* tetrahedron gives (iii)  $N_d \geq N_t$ . We therefore see that (ii) and (iii) imply that those hardcore dimer coverings of the pyrochlore lattice for which each tetrahedron contains exactly one dimer are ground states of the Kivelson-Klein Hamiltonian.

The ensemble of these states maps onto the ground states of the six-vertex model on the diamond lattice,

or equivalently onto the ground states of the pyrochlore Ising antiferromagnet. This can be seen as follows. First, note that the lattice of tetrahedra defined by the pyrochlore lattice is the bipartite diamond lattice. One diamond sublattice sits at the centre of the ‘up’ tetrahedra, the other one at the centres of the ‘down’ tetrahedra. Now let us define the Ising spins on the pyrochlore lattice as follows. For an up (down) tetrahedra, the pair of spins at the two ends of a dimer point up (down), and the other pair points down (up). This defines a one-to-one mapping of dimer to Ising states; crucially, on each tetrahedron, two spins point up and two point down, thus putting the tetrahedron into an Ising ground state. (The mapping to the six-vertex model on the diamond lattice proceeds by calling an up (down) spin an arrow pointing from the centre of an up (down) tetrahedron to a down (up) tetrahedron).

#### 2. Ground state correlations

The total number of ground states (assuming that there are none in addition to the abovementioned dimer states) gives rise to an extensive ground state entropy well-approximated by the Pauling entropy  $\mathcal{S}_{Pauling} = (1/2) \ln(3/2)$ .

Using the mapping to an Ising magnet, it is straightforward to calculate the correlator between singlet bonds averaged over the ground state manifold. To do this, note that each of the six dimer positions on a bond of a given tetrahedron corresponds to an Ising ground state of that tetrahedron. In turn, the corresponding vertex of the six-vertex model describes a net flux, the direction of which is given as follows. Consider a cube circumscribing the tetrahedron in question, so that the bonds of the tetrahedron are face diagonals of the circumscribing cube. The direction of the flux (i.e., the average direction of the four arrows of the given vertex) now points from the centre of the cube through the midpoint of the face of which the bond occupied by the dimer resides.

Using the theory developed in Ref. 12, one can read off that the dimer correlations are simply dipolar. Briefly, this follows from the observation that, upon coarse graining, the smaller the coarse-grained flux, the more microstates (prior to coarse-graining) correspond to it. Modelling this by an effective quadratic weight on the flux configurations leads to simple magnetostatics.

For example, the connected correlator between a pair of dimers located on the top of an up tetrahedra, separated by a vector  $\mathbf{r}$  which makes angle  $\theta$  with the  $z$  axis, is proportional to the dipolar form  $(3 \cos \theta^2 - 1)/r^3$ .

Finally, this model can again in principle be “Rokhsar-Kivelsonized”, i.e. by adding appropriate perturbations to Eq. 5.1, we may generate an effective Hamiltonian which acts on the Kivelson-Klein ground state manifold in a manner similar to Eq. 2.1 on the space of dimer coverings. We do not do this here for a number of reasons. Firstly, the expected phase diagram has the same

topology as that discussed for the diamond lattice in the previous section, so no new phases are obtained. Secondly, the dimer dynamics is rather messy. The shortest resonance loop now involves six dimers straddling a hexagonal loop of the pyrochlore lattice – and there are several symmetry-inequivalent loops of this type. (This is reminiscent of the – exactly soluble – kagome dimer model proposed in Ref. 37.) In addition, for a simple perturbing nearest-neighbour exchange, the resonance term vanishes in the leading order of the overlap expansion, so that a more complex perturbation is needed.

## VI. DISCUSSION AND OUTLOOK

We have presented spin-1/2 Heisenberg Hamiltonians that realize a large class of valence bond phases. In particular they realize  $Z_2$  RVB phases in  $d = 2$  and  $d = 3$ , the  $U(1)$  RVB phase in  $d = 3$  and the Cantor deconfined region in  $d = 2$ . These phases have previously been shown to exist in quantum dimer models with dimers standing in for valence bonds. In this paper we have constructed Klein models that exhibit ground state manifolds spanned by nearest neighbor valence bond states and then perturbed them to realize quantum dimer models within these manifolds. This perturbation is done within the framework provided by the overlap expansion, made arbitrarily accurate by a decoration procedure that we have introduced.

The decoration has the effect of expanding the length scale on which the Hamiltonian acts directly. However in order to stabilize the phases in quantum dimer models, we do not need to go to infinite decoration – it would be enough to suppress subleading terms sufficiently. In this fashion we obtain spin models with interactions of finite range.<sup>44</sup> While large decorations are needed to realize the simplest dimer models under analytic control, there is little reason to doubt that the extent of decoration could be reduced drastically, and even eliminated altogether on some of the lattices without sacrificing the various phases of interest. The subleading interactions will not necessarily uniformly tend to subvert such phases and it is also possible to add other terms that would stabilize them. Showing how this can work is an obvious task for the future, as is the construction of mathematically rigorous proofs for various statements in this paper that are made by appealing to a small parameter. One promising approach is that of Ref. 38, which appeared at the same time as our work, where the phases of the  $d = 2$  bipartite quantum dimer model are realized by perturbing a Klein model with ring exchange terms.

We emphasize that our central result has been the demonstration that spin liquid phases can be realized in  $SU(2)$ -invariant models. However, the actual models we have given involve rather complicated geometries and Hamiltonians without direct experimental relevance. While it may be possible to engineer highly decorated lattices, a more important task perhaps, now that the

question of principle is settled, is to refocus on studying much simpler Hamiltonians. Our insistence on a specified form of the wavefunction (containing nearest neighbor valence bonds alone) has led to fairly complicated Hamiltonians but simpler Hamiltonians can exhibit the same phases with more elaborate ground state wavefunctions. Indeed, the situation for the simplest lattice under consideration in this paper, the (undecorated) honeycomb lattice, looks quite promising. Previous exact diagonalizations of a  $J_1 - J_2 - J_3$  Heisenberg model on this lattice<sup>39</sup> have clearly demonstrated the existence of the staggered VBS. The current data appears not inconsistent with a scenario in which the magnet leaves the staggered phase but never reaches the fluxless plaquette phase. We are optimistic that it will be possible to realize the physics discussed in this paper in such simpler models.

## Acknowledgements

We would like to thank Chris Henley for pointing out to us the pentagonal lattice discussed above. We are very grateful to Steve Kivelson for formulating the generalisation of the Klein model on the pyrochlore lattice. We would like to thank Matt Hastings for a highly stimulating discussion which initiated our thoughts regarding the decoration procedure. We further thank Lincoln Chayes, David Huse and Achim Rosch for useful discussions. RM is grateful to the Aspen Center for Physics, where parts of this work were undertaken. This work was in part supported by the Ministère de la Recherche et des Nouvelles Technologies with an ACI grant. SLS would like to acknowledge support by the NSF (DMR-9978074 and 0213706) and the David and Lucile Packard Foundation.

## APPENDIX A: SIGN CONVENTIONS IN THE OVERLAP MATRIX

In the Rokhsar-Kivelson derivation of the dimer model, the overlap matrix between the different dimer coverings plays a crucial role. Whether or not the RK point corresponds to an equal-amplitude superposition of all dimer coverings depends on the question of whether the dimer Hamiltonian can be turned into a form where all off-diagonal matrix elements are negative.

The leading effect of a perturbing nearest-neighbour exchange finally gives rise to a constant (for each type of loop) multiplying the overlap matrix (restricted to that type of loop). If the overlap matrix can be written as a term proportional to matrix with entries only 0 or 1, the ground state is indeed given by an equal-amplitude superposition at the RK point.

In the following, we demonstrate that a fermionic sign convention may be used to generate the negative sign, independent of lattice details, for models involving valence bond coverings of the lattice. We show that for the honeycomb and diamond lattices, we may obtain the

positive sign as well. We also present a convention for the Kivelson-Klein model which gives the negative sign.

### 1. Overlaps in the fermionic convention

A general convention for overlaps can be obtained by employing the so-called fermionic convention, where a valence bond between sites  $a$  and  $b$  is generated via operators, such as the one placing a fermion with spin up on site  $a$ :  $c_{a\uparrow}^\dagger$ . The singlet bond is then defined as:

$$|[ab]\rangle \equiv d_{ab}^\dagger |0\rangle = \frac{1}{\sqrt{2}}[c_{a\uparrow}^\dagger c_{b\downarrow}^\dagger + c_{b\uparrow}^\dagger c_{a\downarrow}^\dagger] |0\rangle. \quad (\text{A1})$$

Here  $|0\rangle$  is the vacuum state with no fermions present. Note that

$$d_{ab}^\dagger = d_{ba}^\dagger,$$

and that these operators, being bilinear in fermions, commute unless they have exactly one site in common. This means that for constructing a valence-bond covering, the order in which the bonds are generated is inconsequential.

A loop in the transition graph involving sites  $h, i, j$ , and  $k$  will lead to the following type of expression in the overlap matrix element calculation:

$$\begin{aligned} \langle 0 | d_{ab} \cdots d_{ij} d_{jk}^\dagger d_{hi}^\dagger \cdots d_{ab}^\dagger | 0 \rangle \\ = -\frac{1}{2} \langle 0 | d_{ab} \cdots d_{hk}^\dagger \cdots d_{ab}^\dagger | 0 \rangle \end{aligned} \quad (\text{A2})$$

By induction, a loop in the transition graph involving  $L$  dimers in each configuration leads to a factor of  $(-1/2)^{L-1}$ , independently of any further details of the lattice.

### 2. Honeycomb and diamond lattices

The following approach works for both honeycomb and diamond lattice, both of which have a shortest resonance loop of length six, as in the original benzene picture.

As these lattices are bipartite, we can orient each bond to point from one sublattice (A) to the other (B), so that a singlet between sites  $a$  and  $b$  of sublattices A and B, respectively, has the wavefunction

$$|(ab)\rangle \equiv [|\uparrow_a \downarrow_b\rangle - |\downarrow_a \uparrow_b\rangle] / \sqrt{2}. \quad (\text{A3})$$

The two singlet coverings of the benzene loop now have wavefunctions

$$|1\rangle \equiv |(ab)(cd)(ef)\rangle \quad ; \quad |2\rangle \equiv |(bc)(de)(fa)\rangle$$

from which it follows that

$$\langle 1|2\rangle = +1/4 \quad (\text{A4})$$

for any hexagonal plaquette.

It is in fact also possible to choose

$$\langle 1|2\rangle = -1/4 \quad (\text{A5})$$

for the honeycomb lattice. This can, for example, be achieved by choosing any *fixed* hardcore dimer covering of the triangular lattice which is dual to the honeycomb lattice under consideration. One then multiplies each valence bond state of the honeycomb lattice by  $(-1)^{n_\times}$ , where  $n_\times$  is the number of valence bonds which cross dimers of the triangular dimer covering. This generates the desired effect.

### 3. Other bipartite lattices

The above construction for generating uniform overlap matrix elements can be generalised to any bipartite lattice. By orienting the bonds from one sublattice to the other, one always obtains an overlap which is positive; its size is the simple product over the individual loops involved in the transition graph.

$$\langle k|l\rangle > 0; \quad (\text{A6})$$

indeed, the positive overlap holds true for any value of the loop length, and therefore for an arbitrary pair of valence bond coverings  $|k\rangle, |l\rangle$ .

### 4. Kivelson-Klein model on pyrochlore lattice

Here we first need to establish the possible resonance loops. These involve six dimers on a cluster of twelve sites arranged as follows.

Six of the sites sit on a hexagonal ring on the pyrochlore lattice; each link of this hexagonal ring belongs to a different tetrahedron. Each of these six tetrahedra contains one dimer linking a site on the hexagonal ring with a site off the hexagonal ring. As there is a choice of 2 such off-sites per tetrahedron, the total number of shortest resonance loops corresponding to each hexagonal ring equals  $2^6 = 64$ . Not all of these loops are symmetry equivalent.

These loops all involve moving six dimers. Hence, their overlap in the Fermion convention is given by  $-1/32$ .

## APPENDIX B: SPINON GAP FOR THE DECORATED HONEYCOMB LATTICE

A stable RVB liquid phase requires not only certain properties of the ground state wavefunction but also that the excitation spectrum has a lower bound. In this section, we argue that the nearest neighbor valence bond ground states are separated by a finite gap from the excited states for the case of the decorated honeycomb lattice Klein model.

To this end observe that in the highly decorated limit we are connecting a set of Majumdar-Ghosh<sup>7</sup> (MG) chains into a two-dimensional network. The excitations of the chains themselves are well studied: these are spinon defects between the two different dimerizations and there is considerable analytical<sup>29,30</sup> and numerical<sup>31</sup> evidence that they are gapped. In putting the chains together we need to ask if the intersections lead to the emergence of states *below* the one-spinon continuum on the chains that can fill in the gap. In the infinite decoration limit, it is sufficient to consider a single intersection: thus we look for bound states localized near a site of the original honeycomb lattice where three MG chains would cross (see Fig. 11).

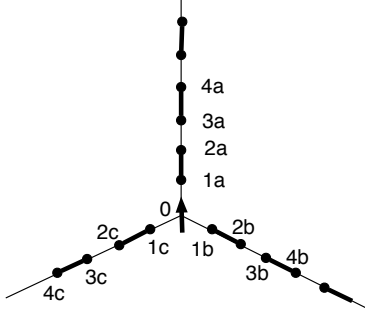


FIG. 11: This figure depicts a spinon at the crossing of the edges of a decorated honeycomb lattice.

We consider a variational wavefunction describing a single spin at the crossing of three semi-infinite MG chains.

$$|\psi\rangle_0 = |+\rangle_0 |00\rangle_{ee} \quad (B1)$$

where  $|+\rangle_0$  denotes an up spin at location 0 and  $|00\rangle_{ee}$  denotes that “everything else” is dimerized into singlet (00) pairings. We consider the action of the Klein Hamiltonian (3.1) on this state. Observe that  $\hat{P}_{N(0)}$ , which involves only site 0 and its three neighbors, is the only projector that does not destroy our trial function. A standard calculation gives:

$$\hat{P}_{N(0)}|\psi\rangle_0 = C_{cr} \left[ \frac{54}{4} |\psi\rangle_0 + 4(|\psi\rangle_{2a} + |\psi\rangle_{2b} + |\psi\rangle_{2c}) + |\alpha\rangle \right] \quad (B2)$$

where  $|\psi\rangle_i = |+\rangle_i |00\rangle_{ee}$  describes an up spin at location  $i$  with everything else paired into singlets and  $C_{cr}$  sets the energy scale for violating the Klein condition at the cross. We can also compute the effect of operator (3.1) on the state  $|\psi\rangle_i$ , where  $i$  is a location along a chain; in this case, only  $\hat{P}_{N(i)}$  contributes:

$$\hat{P}_{N(i)}|\psi\rangle_i = C_{ch} \left[ \frac{5}{2} |\psi\rangle_i + |\psi\rangle_{i-2} + |\psi\rangle_{i+2} + |\beta\rangle \right] \quad (B3)$$

Here  $C_{ch}$  is the energy scale for violating the Klein condition on the chain. We see that the Klein Hamiltonian

acting on a spinon state produces the original state along with states where the spin has hopped two sites. We also obtain terms which are orthogonal to all spinon states, designated here by the expressions  $|\alpha\rangle$  and  $|\beta\rangle$ . This motivates the bound state trial function:

$$|\psi\rangle = |\psi\rangle_0 + \sum_{n>0; i=a,b,c} y^n |\psi\rangle_{2n,i} \quad (B4)$$

where  $y$  is a variational parameter less than unity. In calculating the expectation of the energy, we need to contend with the non-orthogonality of the spinon states:

$${}_i\langle\psi|\psi\rangle_j = \left(-\frac{1}{2}\right)^{|i\pm j|/2} \quad (B5)$$

for sites  $i$  and  $j$  on the same (different) chain(s). A tedious but standard calculation<sup>40</sup> gives the expectation value for the energy of the trial state (B4):

$$E = \frac{\langle\psi|H_K|\psi\rangle}{\langle\psi|\psi\rangle} \quad (B6)$$

$$\begin{aligned} \frac{\langle\psi|H_K|\psi\rangle}{C_{cr}} &= \frac{30+6a}{4} + 3ay \\ &+ \left[ \frac{18+66a}{4} + \frac{3a}{y} + 12ay \right] \left[ \frac{-y/2}{1+y/2} \right] \\ &+ \left[ \frac{5a}{2} + \frac{a}{y} + ay \right] \left[ 6 \left( \frac{-y/2}{1+y/2} \right)^2 \right] \\ &+ \frac{3y^2(1-y/2)}{(1+y/2)(1-y^2)} \end{aligned} \quad (B7)$$

$$\begin{aligned} \langle\psi|\psi\rangle &= 1 + 6 \frac{-y/2}{1+y/2} + 6 \left( \frac{-y/2}{1+y/2} \right)^2 \\ &+ \frac{3y^2(1-y/2)}{(1+y/2)(1-y^2)} \end{aligned} \quad (B8)$$

where  $a = C_{ch}/C_{cr}$ .

Fig. 12 shows a graph of this expression for several values of  $a$ . For small values of  $a$ , the spinon wavefunction is an extended scattering state while for large values, the wavefunction is localized at the cross.

Our analysis has been for the infinite decoration limit. For large, but finite, decoration, the extended spinon states obtained for small  $a$  may be interpreted as MG spinons scattering at the vertices. In this limit, the natural extension of the localized states obtained for large  $a$  will involve the wavefunction having peaks at the reference sites and decaying on the chains. There will be a band of such localized states below the scattering states. We may estimate the bandwidth by considering a variational wavefunction where the spinon resides only on the reference sites:

$$|\Psi\rangle = \sum_{\vec{n}} e^{i\vec{k}\cdot\vec{n}} |\vec{n}\rangle \quad (B9)$$

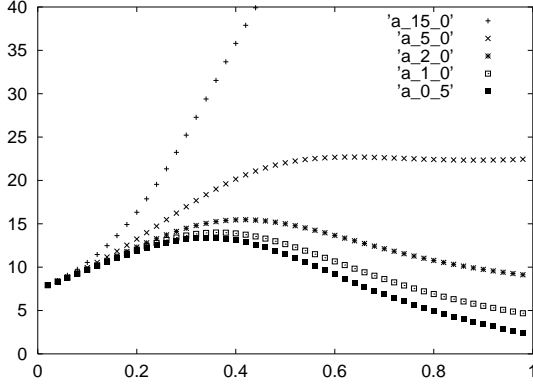


FIG. 12: This plot gives the energy expectation as a function of the variational parameter  $y$  for different values of  $a = C_{ch}/C_{cr}$ , which is ratio of Klein scales; the energy is measured in units of  $C_{cr}$ . For large values of this ratio, the minimum occurs for  $y = 0$  which corresponds to spinons localized at the crossing. For small values, the minimum occurs at  $y = 1$ , which is an extended spinon state. At a value slightly greater than  $a = 1$ , there is a first order “phase transition” between these limits. The important feature is that for any nonzero  $a$ , there is an energy gap between spinon states and the valence bond states, which have zero energy.

where  $|\vec{n}\rangle$  denotes a wavefunction of the form (B1) for the spinon at lattice site  $\vec{n}$ . The variational energy of this trial state, to leading order in a large  $N$  expansion, where  $N$  is the number of sites inserted between reference sites in the decoration, is given by:

$$E = C_{cr} \left[ \frac{54}{4} + 16x^{2N} \left( \cos k_x + \cos\left(\frac{k_x}{2} + \frac{\sqrt{3}k_y}{2}\right) + \cos\left(\frac{k_x}{2} - \frac{\sqrt{3}k_y}{2}\right) \right) \right] \quad (\text{B10})$$

where  $x = \frac{1}{\sqrt{2}}$ . We see that the band becomes more narrow as the decoration is increased.

In our analysis so far, we have considered states where the defects are always an even number of sites away from the reference sites. There is another family of spinon states corresponding to the defects being located on the odd sites. Referring to Fig. 13, the Klein operator permits the spin at 1a to hop only to the site 1b, which is connected by a dimer to the origin. Therefore, in the large decoration limit, this is equivalent to the MG chain, which we know is gapped.

### APPENDIX C: RESULTS FOR THE PENTAGONAL LATTICE

At infinite temperatures, where “infinite” means a temperature that is small compared with the excitation gap of the Klein Hamiltonian but much larger than

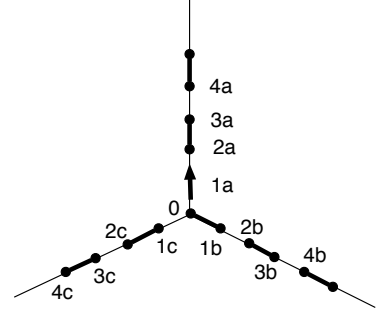


FIG. 13: This shows a representative of the family of states where a spinon is an odd distance from the origin. In this configuration, the Klein operator may hop the spinon only onto the  $b$ -chain. The configuration where the origin forms a singlet with 1c is essentially orthogonal to the given configuration for large decoration.

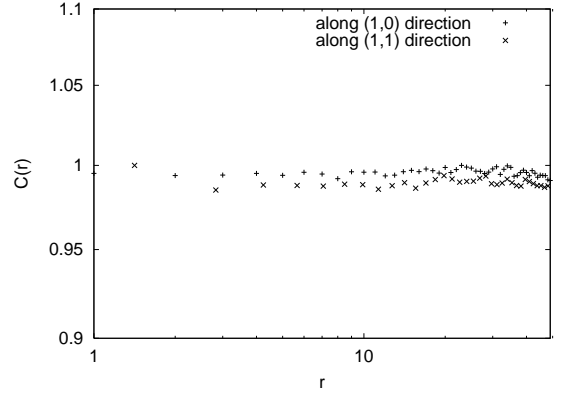


FIG. 14: The monomer-monomer correlation function for a  $100 \times 100$  pentagonal lattice with periodic boundary conditions. The two curves are cuts along the  $\hat{x}$  and  $\hat{x} + \hat{y}$  directions. The distance  $r$  refers to the distance between unit cells. In computing these correlation functions, we take the two test monomers to be on the same sublattice (the pentagonal lattice is a cubic lattice with a six point basis). Each data point is an average over  $N = 10^6$  data points and the noise seen in the plot is of the order of Monte Carlo noise  $1/\sqrt{N} \sim 10^{-3} \sim 0.1\%$ .

the energy scales of the quantum dimer Hamiltonian, the dimers are described classically, i.e. thermodynamic quantities are computed as equal-weight averages over all dimer states. The number of dimer states grows exponentially with lattice size. This number may be computed using the method of Kasteleyn.<sup>41,42</sup> The results are shown in table I. The method also yields the entropy per site in the thermodynamic limit.

$$S = 0.168608 \dots \quad (\text{C1})$$

The striking feature of table I is that even fairly small systems have an enormous number of dimer coverings

$L_x$	$L_y$	$n_d$
1	1	4
2	1	12
3	1	28
4	1	68
5	1	164
6	1	396
1	2	12
2	2	136
3	2	1068
4	2	9488
5	2	86252
6	2	798856
1	3	28
2	3	1068
3	3	17836
4	3	373412
5	3	7732928
6	3	160648524
1	4	68
2	4	9488
3	4	373412
4	4	21643648
5	4	1235195428
6	4	70937630864
1	5	164
2	5	86252
3	5	7732928
4	5	1235195428
5	5	192674444864
6	5	30315148743302
1	6	396
2	6	798856
3	6	160648524
4	6	70937630864
5	6	30315148743302

TABLE I: Table of the number of dimer configurations for an  $L_x \times L_y$  size pentagonal lattice. Here  $L_x$  and  $L_y$  refer to the underlying square lattice; the pentagonal lattice is a square lattice with a 6 point basis. We have assumed periodic boundary conditions in this calculation.

so numerical studies of large systems require Monte-Carlo simulations. Fig. 14 is a Monte-Carlo calculation of monomer-monomer correlation functions  $C(r)$  for the pentagonal lattice using the algorithm of Sandvik<sup>43</sup>.  $C(r)$  is defined as the number  $n_d(r)$  of dimer coverings given a pair of test monomers separated by distance  $r$  divided by  $n_d(1)$ . The simulation shows monomer deconfinement at infinite temperatures, as opposed to the square and honeycomb lattices which show logarithmic confinement. This indicates a liquid phase at high temperatures. The RK point also has deconfined monomers and the same dimer correlations as the high temperature phase, which strongly suggests that the RK point is part of a zero temperature liquid phase which connects continuously to the high temperature liquid.

- 
- <sup>1</sup> P. Fazekas and P. W. Anderson, Philos. Mag. **30**, 23 (1974)  
<sup>2</sup> P. W. Anderson, Science **235**, 1196 (1987).  
<sup>3</sup> T. H. Hansson, V. Oganesyan, and S. L. Sondhi, Annals Of Physics **313**, 497 (2004).  
<sup>4</sup> S. A. Kivelson, D. S. Rokhsar, and J. P. Sethna, Phys. Rev. B **35**, R8865 (1987).  
<sup>5</sup> See P. W. Anderson, P. A. Lee, M. Randeria, T. M. Rice, N. Trivedi and F. C. Zhang, J Phys. Condens. Matter **16**, R755 (2004) and P. A. Lee, N. Nagaosa and X.-G. Wen, cond-mat/0410445 for recent reviews.  
<sup>6</sup> M. Hermele, T. Senthil, M. P. A. Fisher, P. A. Lee, N. Nagaosa, X.-G. Wen, Phys. Rev. B **70**, 214437 (2004).  
<sup>7</sup> C. K. Majumdar and D. K. Ghosh, J. Math. Phys. **10**, 1388 (1969)  
<sup>8</sup> H. Bethe, Z. Phys. **71**, 205 (1931).  
<sup>9</sup> D. A. Huse and V. Elser, Phys. Rev. Lett. **60**, 2531 (1988); B. Bernu, P. Lecheminant, C. Lhuillier, and L.

- Pierre, Phys. Rev. B **50**, 10048 (1994); L. Capriotti, A. E. Trumper, and S. Sorella, Phys. Rev. Lett. **82**, 3899 (1999).  
<sup>10</sup> D. S. Rokhsar and S. A. Kivelson, Phys. Rev. Lett. **61**, 2376 (1988).  
<sup>11</sup> R. Moessner and S. L. Sondhi, Phys. Rev. Lett. **86**, 1881 (2001).  
<sup>12</sup> D. A. Huse, W. Krauth, R. Moessner, and S. L. Sondhi, Phys. Rev. Lett. **91**, 167004 (2003).  
<sup>13</sup> R. Moessner and S. L. Sondhi, Phys. Rev. B **68**, 184512 (2003).  
<sup>14</sup> M. Hermele, M. P. A. Fisher, L. Balents, Phys. Rev. B **69**, 064404 (2004)  
<sup>15</sup> E. Fradkin, D. A. Huse, R. Moessner, V. Oganesyan, and S. L. Sondhi, Phys. Rev. B **69**, 224415 (2004). See also: A. Vishwanath, L. Balents, and T. Senthil, Phys. Rev. B **69**, 224416 (2004).  
<sup>16</sup> J. T. Chayes, L. Chayes, and S. A. Kivelson, Commun.

- Math. Phys. **123**, 53 (1989).
- <sup>17</sup> D. J. Klein, J. Phys. A: Math. Gen. **15**, 661 (1982).
  - <sup>18</sup> N. Read and S. Sachdev, Phys. Rev. Lett. **66**, 1773 (1991). O. Tchernyshyov, R. Moessner, and S. L. Sondhi, cond-mat/0408498.
  - <sup>19</sup> see e.g.: P. W. Anderson, P.A. Lee, M. Randeria, T.M. Rice, N. Trivedi, and F. C. Zhang, J. Phys. Cond. Mat. **16**, R755 (2004). L. Arrachea, L. Capriotti, S. Sorella, Phys. Rev. B **69**, 224414 (2004).
  - <sup>20</sup> G. Misguich, B. Bernu, C. Lhuillier and C. Waldtmann, Phys. Rev. Lett. **81**, 1098 (1998).
  - <sup>21</sup> G. Misguich and C. Lhuillier, *Frustrated spin systems*, H.T. Diep, editor, World-Scientific (2005); also available as cond-mat/0310405. See also a subsequent DMRG study: L. Capriotti, D. J. Scalapino, S. R. White, Phys. Rev. Lett. **93**, 177004 (2004).
  - <sup>22</sup> A. Y. Kitaev, Annals Of Physics **303**, 2 (2003).
  - <sup>23</sup> R. Coldea, D.A. Tennant, A.M. Tsvelik, and Z. Tylczynski, Phys. Rev. Lett. **86**, 1335 (2001).
  - <sup>24</sup> Y. Shimizu, K. Miyagawa, K. Kanoda, M. Maesato, and G. Saito, Phys. Rev. Lett. **91**, 107001 (2003).
  - <sup>25</sup> M. Mambrini, *private communication*.
  - <sup>26</sup> Historically, Rokhsar and Kivelson were motivated to consider restricting the dynamics of the nearest neighbor antiferromagnet on the square lattice to the valence bond manifold. This Hamiltonian is now known to have long range order. We will consider considerably more frustrated Hamiltonians.
  - <sup>27</sup> R. Moessner, S. L. Sondhi and P. Chandra, Phys. Rev. B **64**, 144416 (2001).
  - <sup>28</sup> We could, in principle, select a perturbation to generate a more complex term at lower order in the overlap expansion described in section IIIB.
  - <sup>29</sup> B. S. Shastry and B. Sutherland, Phys. Rev. Lett. **47**, 964 (1981)
  - <sup>30</sup> W. J. Caspers, K. M. Emmett, and W. Magnus, J. Phys. A: Math. Gen. **17**, 2687 (1984).
  - <sup>31</sup> E. Sorensen, I. Affleck, D. Augier, and D. Poilblanc, Phys. Rev. B **58**, R14701 (1998).
  - <sup>32</sup> R. Moessner and S. L. Sondhi, Progr. Theor. Phys. Suppl. **145**, 37 (2002)
  - <sup>33</sup> D. A. Ivanov, Phys. Rev. B **70**, 094430 (2004).
  - <sup>34</sup> In a previous paper, we have used the name pentagonal lattice for a different tiling of the plane with irregular pentagons. As all the pentagons in the lattice under consideration in this paper are equivalent, we feel it is more appropriate to use the name pentagonal lattice here.
  - <sup>35</sup> J. F. Nagle, Phys. Rev. **152**, 190 (1966) J. F. Nagle, J. Math. Phys. **7**, 1484 (1966)
  - <sup>36</sup> This model is named in honor of S. Kivelson, who formulated this generalization of the Klein model on the pyrochlore lattice. A model of this type on the square lattice has been studied by Kivelson (unpublished) and recently by C. Batista and S. A. Trugman, Phys. Rev. Lett. **93**, 217202 (2004).
  - <sup>37</sup> C. Zeng and V. Elser, Phys. Rev. B **51**, 8318 (1995). G. Misguich, D. Serban, V. Pasquier, Phys. Rev. B **67**, 214413 (2003). G. Misguich, D. Serban, V. Pasquier, J. Phys. Cond. Mat. **16**, 823 (2004).
  - <sup>38</sup> S. Fujimoto, cond-mat/0501698
  - <sup>39</sup> J.-B. Fouet, M. Mambrini, Ph. Sindzingre and C. Lhuillier, Phys. Rev. B **67**, 054411 (2003).
  - <sup>40</sup> K. S. Raman, Ph.D. Thesis *in preparation*
  - <sup>41</sup> P. W. Kasteleyn, Physica **27**, 1209 (1963). P. W. Kasteleyn, J. Math. Phys. **4**, 287 (1963).
  - <sup>42</sup> P. Fendley, R. Moessner, and S. L. Sondhi, Phys. Rev. B **66**, 214513 (2002).
  - <sup>43</sup> A. W. Sandvik, cond-mat/0312097
  - <sup>44</sup> In the Cantor deconfined region matters are more delicate since it involves a Cantor set of critical states. Nevertheless, the general argument in Ref. 15 required only the weakness of a generic perturbation so that should still go through.